Re-examination of the Maximum Normalized Vortex-Induced Side Force

J. Peter Reding* and Lars E. Ericsson†
Lockheed Missiles & Space Company, Sunnyvale, California

A critical review of recent experimental data tends to confirm the validity of previously published asymmetric flow concepts: 1) That the maximum side force to normal force ratio (the maximum normalized side force) on slender bodies of revolution at high angles of attack and zero sideslip occurs in the critical Reynolds number range where the maximum local flow separation asymmetry can occur; 2) that body motion can lock in a driving vortex asymmetry to produce self-induced body coning; and 3) that laminar vortex separation may occur on the cylinder of an ogive-cylinder at high angles of attack, even when the nose experiences turbulent separation. In addition, the present analysis offers a realistic explanation as to why a minimum normalized side force is realized at a Reynolds number slightly above that for the maximum normalized side force.

Nomenclature

c = reference length, $c = d$
d = maximum diameter for body of revolution
$\bar{d}$ = mean diameter = $(2/\ell)\int_0^\ell r\,dx$
d' = sectional drag: coefficient $c_d = d/(\rho_\infty U_\infty^2/2)c$
f = vortex shedding frequency
l = sectional lift: coefficient $c_l = 1/(\rho_\infty U_\infty^2/2)c$
ℓ = total body length
M = freestream Mach number
N = normal force: coefficient $C_N = N/(\rho_\infty U_\infty^2/2)S$
n = sectional normal force: coefficient $c_n = n/(\rho_\infty U_\infty^2/2)c$
P = static pressure: coefficient $C_p = (p - p_\infty)/(\rho_\infty U_\infty^2/2)$
P_b = base pressure: coefficient $C_{p_b} = (p_b - p_\infty)/(\rho_\infty U_\infty^2/2)$
r = body radius
r_N = nose radius
$R_{\bar{d}}, R_d$ = Reynolds number = $U_\infty \bar{d}/\nu_\infty$ or $U_\infty d/\nu_\infty$
R_{eff} = effective Reynolds number
S = reference area = $\pi c^2/4$
U_∞ = freestream velocity
x = axial coordinate
Y = side force: coefficient $C_Y = Y/(\rho_\infty U_\infty^2/2)S$
y = sectional side force: coefficient $c_y = y/(\rho_\infty U_\infty^2/2)c$
α = angle of attack
β = angle of sideslip
ν_∞ = freestream kinematic viscosity
ρ_∞ = freestream air density
φ = roll angle
ω = spin rate

Subscripts

eff = effective
max = maximum
p = peak amplitude
RMS = root-mean-square

Presented as Paper 83-0458 at the AIAA 21st Aerospace Sciences Meeting, Reno, Nev., Jan. 10-13, 1983; submitted Feb. 24, 1983; revision received Sept. 14, 1983.

*Staff Engineer. Associate Fellow AIAA.
†Senior Consulting Engineer. Associate Fellow AIAA.

Introduction

A FEW years ago the present authors presented a method[1,2] for bounding the vortex-induced side force to normal force ratio (the normalized side force) on slender bodies. This was needed to aid the designer in establishing control power requirements because of the lack, then as now, of any theoretical or experimental means to reliably predict the vortex-induced side force. The method was based on the widely held hypothesis that the stationary asymmetric vortex wake behind slender bodies at high angles of attack was in essence similar to the unsteady asymmetric vortex wake of a two-dimensional (2D) cylinder. It was postulated that the axial flow component enabled the vortices shed from the three-dimensional (3D) body to stabilize in a steady asymmetric configuration. Thus, the sectional side force to normal force ratio was related to the sectional unsteady lift to drag ratio on a two-dimensional cylinder. The peak unsteady lift to steady drag ratio for the 2D cylinder was defined from the literature. Comparisons with 3D slender body data verified that the maximum sectional side force to normal force ratio on a slender body was bounded by the maximum unsteady 2D lift to drag ratio.

It was also shown that the maximum local, normalized side force occurred in a Reynolds number region where the maximum local flow separation asymmetry could be established. Recent experimental results are in agreement with this finding, and have also revealed that a minimum normalized side force occurs when the Reynolds number is increased slightly.

The authors also postulated that the vehicle motion could couple with the vortex shedding to lock in the maximum flow separation asymmetry. We additionally speculated that relaminarization could cause laminar vortex separation to occur on the cylinder of an ogive-cylinder even though turbulent separation existed on the nose.[3-5] Experimental data have now become available that confirm the postulated effects of body motion and that indicate that there may be a degeneration of the flow separation type from turbulent to laminar along a slender nose-cylinder body at high angles of attack.

The 2D Cylinder Analogy

In our earlier work, an effective crossflow Reynolds number (R_{eff}) was developed from potential flow theory that could define the character of the separation (laminar or turbulent) verified by the superior collapse of Clark's crossflow drag data.[2,7,8] At angles of attack above 30 deg, the effective Reynolds number on a cylinder is essentially equal to the crossflow Reynolds number (i.e., $R_{\text{eff}} = R_d$).[9] Thus, the sectional characteristics for the slender body should be similar to those of a 2D cylinder. Hence, the maximum sectional 3D

normalized side force should be analogous to the peak lift to drag ratio of a 2D cylinder,

$$c_y/c_n = c_{lp}/c_d \quad (1)$$

In the past, we have referred to the entire Reynolds number region above subcritical (laminar flow separation) range as being supercritical. In order to describe the varied flow phenomena that occur at Reynolds numbers above the subcritical range more accurately, it is necessary to be more precise. Following Achenbach's terminology,[10] a cylinder in incompressible crossflow experiences four distinct flow regimes, each with a different type of flow separation, as is sketched in Fig. 1. At subcritical Reynolds numbers, the boundary layer is laminar, and flow separation occurs near the lateral meridian ($\varphi = 80$ to 90 deg). In the critical Reynolds number range, a laminar separation bubble develops near the lateral meridian ($\varphi = 90$ deg) followed by transition in the lifted layer and turbulent reattachment. The reattached turbulent boundary layer is more energetic than the laminar boundary layer, and separation is delayed, resulting in a dramatic reduction of the drag.

The laminar bubble and following turbulent reattachment is similar to the preseparation effect which is so effective in delaying downstream flow separation.[11] In the present case, the reattaching shear flow delays the wake separation to $\varphi = 140$ deg (critical flow region), which is well aft of the final transcritical location of $\varphi = 100$ deg.[12] Thus, a drag bucket is produced in the critical Reynolds number region (Fig. 1).

As the Reynolds number is increased, transition moves forward of the lateral meridian, and the laminar bubble with its beneficial effect on separation is lost. Thus, separation moves forward of $\varphi = 140$ deg and reaches the final transcritical value of $\varphi = 100$ deg as the turbulent boundary layer thickness grows with increasing Reynolds number. A drag increase, of course, accompanies the wake growth.

Ordinarily one would expect that discontinuous changes in the drag would occur as the laminar bubble develops and collapses suddenly. However, three-dimensional flow effects cause the development and collapse of the laminar bubble to occur in finite cells.[13,14] Through spanwise communication effects[15] the cells finally coalesce to form a continuous bubble across the span of the cylinder.

The peak sectional lift force on a cylinder normal to the flow occurs at a Reynolds number where the maximum flow separation asymmetry exists.[16,17] It should be noted that in the past we have used the term supercritical separation to denote any type of turbulent separation. Here we are making a distinction between critical, supercritical, and transcritical separation to describe in more detail the flow phenomenon responsible both for the maximum and minimum normalized side force. Both supercritical and critical separation allow large suction peaks to be realized on one side of the body; whereas, on the other side, subcritical separation cuts off the peak suction pressures, producing a large pressure differential across the body. The pressure drops sharply as the separation moves rearward in the critical Reynolds number range, resulting in a pronounced maximizing of the 2D lift to drag ratio. Static measurements of this separation asymmetry[16,17] were used, along with unsteady c_{lRMS} and c_{lp} results from the literature, to define the envelope of c_{lp}/c_d over the entire Reynolds number range.[1,2]

The Reynolds number of the critical flow condition can vary drastically from one test to another and from one wind tunnel to another due to the effects of tunnel turbulence level, boundary layer noise, body motion, and roughness (Fig. 2).[14] The maximum c_l/c_d that occurs due to critical/subcritical separation was spread over the entire critical Reynolds number range as defined by Humphreys' data[15] since, depending on wind tunnel turbulence, body roughness, or body dynamics (to be discussed later), this condition could occur anywhere within this Reynolds number range.

Unpublished pressure data by Dahlem et al.[18] show that this critical/supercritical separation occurs on 3D bodies at high angles of attack[2] (Fig. 3). At $x/d = 6.1$, subcritical flow separation occurs on one side of the body (at $\varphi = 80$ deg) and critical separation on the other (at $\varphi = 225$ deg or 135 deg aft of the windward ray). This 3D flow separation is in agreement with experimental results for 2D cylinders[19] (Fig. 3). At $x/d = 8.75$, subcritical/critical separation still occurs but the subcritical peak has been reduced greatly, falling approximately 40% below the 2D value. It can be noted further that the vortex asymmetry develops gradually, forming a roughly triangular distribution along the body within a single cell.[2] A cell ends when a vortex is shed to reverse the vortex asymmetry, thus reversing the sign of the side force (inset in Fig. 4). Thus,

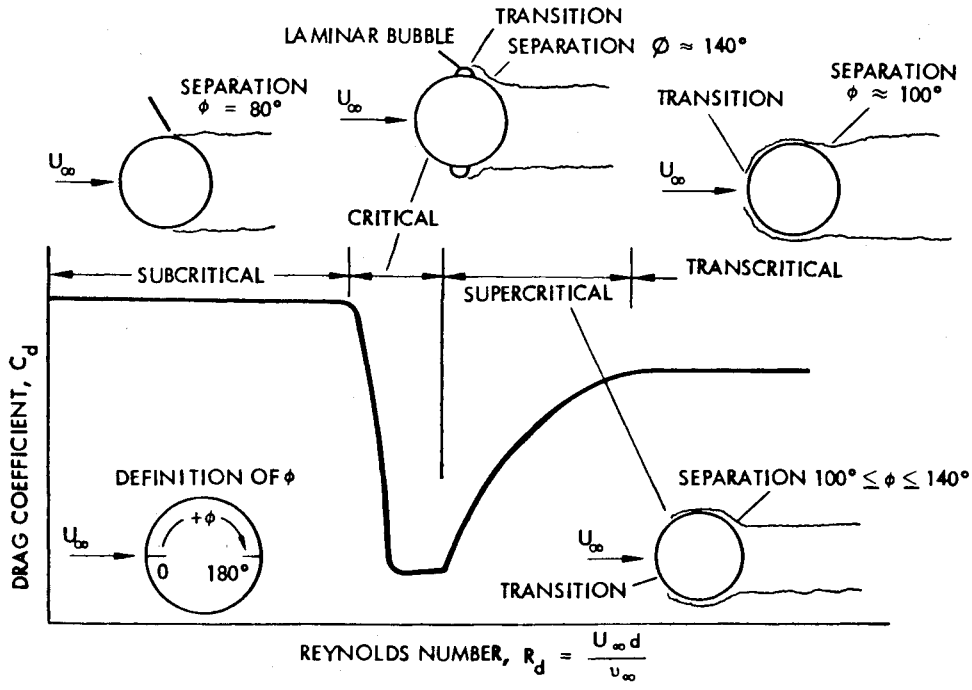

Fig. 1 Flow regions for a circular cylinder.

the maximum side force within a single cell should be approximately half of the peak sectional value. (Use was also made of the triangular side force distribution to predict the center of pressure of the side force.[2])

$$|C_Y|_{max}/C_N = 0.5(c_y/c_n) = 0.5(c_{\ell p}/c_d) \qquad (2)$$

By using the effective Reynolds number, one can predict the body normal force from the crossflow analogy,[20] and from the variation of $|C_Y|_{max}/C_N$ with R_{eff}, the corresponding maximum side force can be determined. It should be emphasized that while the maximum normalized side force, $|C_Y|_{max}/C_N$, has been implicitly derived for a body dominated by a single asymmetric vortex pair (a single cell), it also bounds the maximum side force for bodies with multiple alternating vortex pairs which produce opposing left-right side force cells that tend to cancel one another. Even though the side force can be conservatively bounded for long bodies using this technique, the moment cannot. Thus, the method of Ref. 2 cannot, for practical purposes, be applied to long bodies.

The peak $|C_Y|_{max}/C_N$ always occurs in the critical Reynolds number range where the body can experience subcritical/critical vortex separation. Surprisingly, the maximum total side force does not necessarily occur at the same critical Reynolds number even though the body is experiencing the maximum lateral pressure differential locally. This is because the length of the first side force cell shrinks in the critical Reynolds number range (Fig. 4).[18,20,21] Thus, it is theoretically possible for the maximum side force to occur at a Reynolds number different from that giving the peak normalized side force.

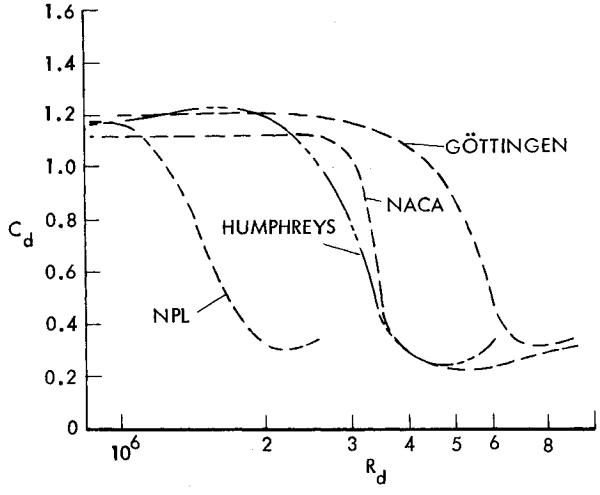

Fig. 2 Drag coefficient vs Reynolds number in different ground facilities (Ref. 15).

Recent Experimental Results

The data of Keener et al.[22-26] for pointed ogives ($\ell/d = 3.5$ and 5.0) fell along the upper boundary of our $|C_Y|_{max}/C_N$ curve. This, we reasoned, was because these bodies when experiencing subcritical/critical flow separation, were dominated by a single side force cell and, therefore, experienced the peak $|C_Y|_{max}/C_N$. Keener has recently published oil flow data which show subcritical, critical, and supercritical vortex separation (laminar, transitional, and turbulent separations, respectively, in Keener's terminology) occurring on an $\ell/d = 3.5$ pointed ogive.[27] An example of this can be seen in Keener's oil flow sketch for $\varphi = 55$ deg where C_Y is a maximum (Fig. 5). Critical separation occurs on the right side of the ogive aft of about 20% of length, as is indicated by the existence of a laminar separation bubble followed by turbulent separation (Keener's transitional separation). On the left side subcritical (Keener's laminar) separation occurs back to about 40% of length. Although Keener presents only side force measurements along with the oil flows, these measurements are in good agreement with earlier side force data.[26] If the normalized side force is in equally good agreement, then this is also the condition where $|C_Y|_{max}/C_N$ occurs. Thus, the maximum normalized side force is associated with critical/subcritical separation being present over a significant portion of the body length.

Because the critical Reynolds number can vary so drastically depending upon facility and model idiosyncrasies (Fig. 2), one needs some positive indication of the location of flow separation (e.g., flow visualization results, or pressure mea-

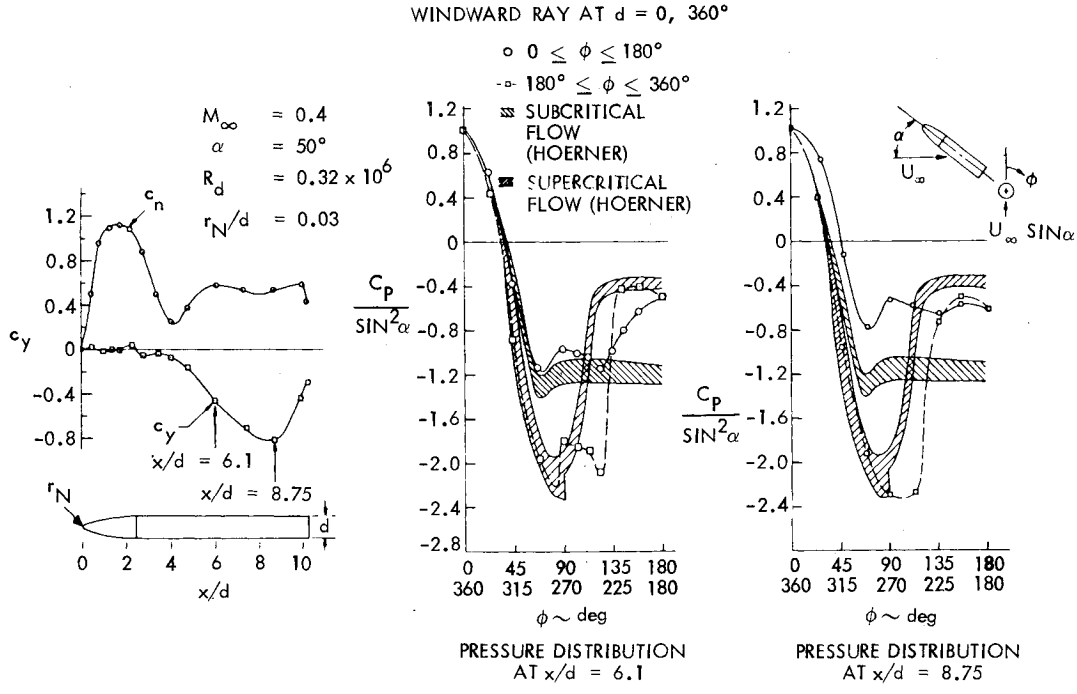

Fig. 3 Evidence of subcritical/critical vortex separation as a slender body.

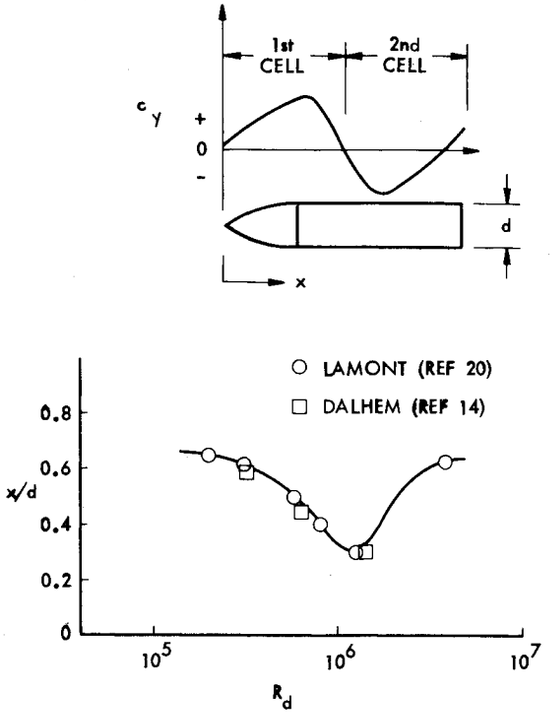

Fig. 4 Contraction of first vortex induced side force cell in the critical Reynolds number range.

surements) to determine the separation state conclusively.

It should once again be emphasized that our $|C_Y|_{max}/C_N$ boundary was derived for bodies dominated by a single side force cell. Three recent papers,[21,29,30] one of which is a review paper, have missed this point entirely. Both authors use $C_{Y_{max}}$ measurements on bodies dominated by opposing left-right side force components (multiple cells) to refute our postulations. For example, Lamont[21] presents $|C_Y|_{max}$ data for an $\ell/d = 6.0$ ogive-cylinder that exhibit a minimum $|C_Y|_{max}$ for $0.8 \times 10^6 \leq R_d \leq 1.2 \times 10^6$ (Fig. 6). The force distributions show that a second, opposite side force cell develops over the cylindrical afterbody (in the critical Reynolds number range), which is the cause of the measured C_Y minimum[29] (Fig. 7). Other force measurements are also indicative of the develop-

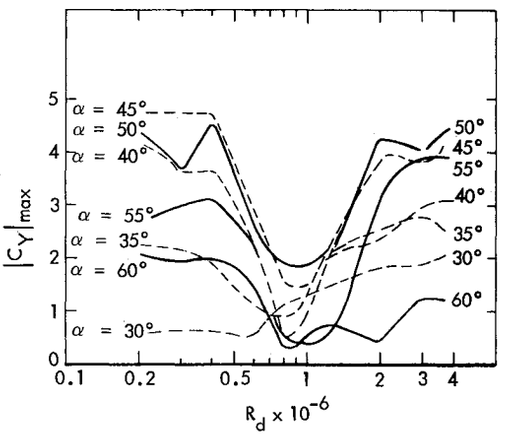

Fig. 6 Variation of maximum side force with R_d at various angles of attack (Ref. 29).

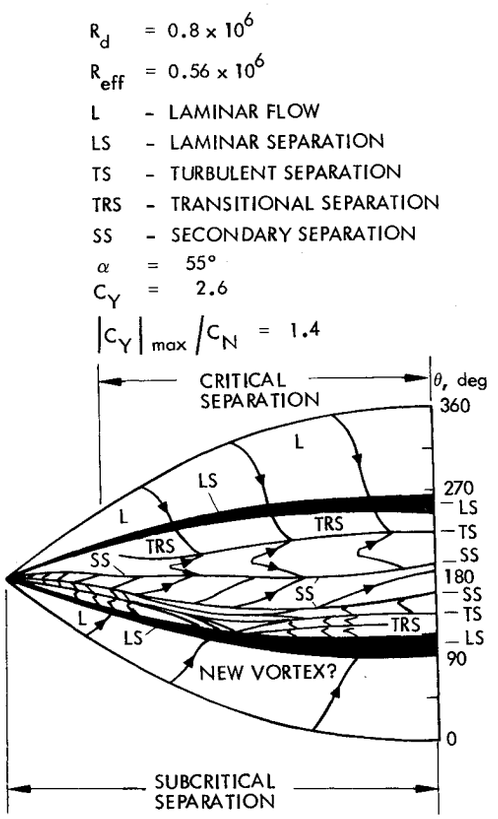

Fig. 5 Flow patterns near maximum $|C_Y|/C_N$ and $|C_Y|$ for an $\ell/d = 3.5$ pointed ogive (Ref. 27).

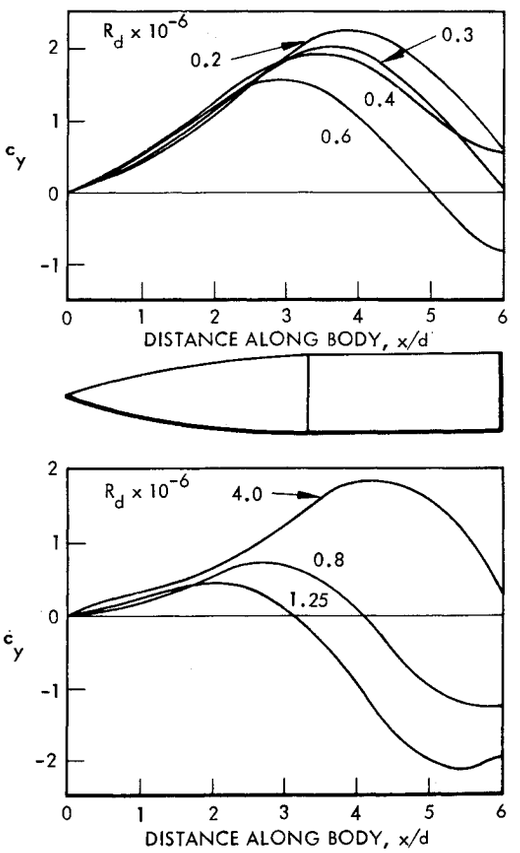

Fig. 7 Side force distributions on an ogive-cylinder, $\ell/d = 6.0$, $\alpha = 40$ deg (Ref. 29).

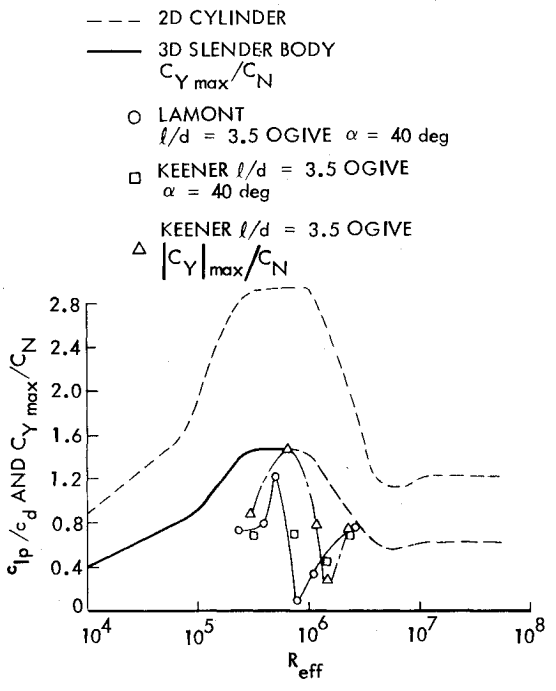

Fig. 8 Maximum normalized side force.

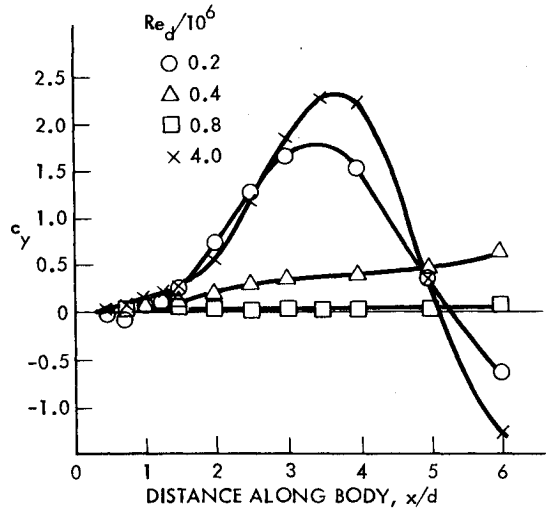

Fig. 9 Side force distributions at different Reynolds numbers, $\alpha = 55$ deg (Ref. 21).

ment of an opposing side force component on a cylinder aft of a similar $\ell/d = 3.5$ pointed ogive.[23] Thus, one needs to examine the side force of the first cell to test the validity of our postulation. Unfortunately, Lamont does not present load distributions for the $C_{Y\max}$ conditions so one cannot determine at which Reynolds number the peak, single cell $|C_Y|_{\max}/C_N$ occurs. It is interesting to note, however, that when the $|C_Y|_{\max}/C_N$ ratio is formed from the $\varphi = 40$ deg distributions for the ogive alone, it tends to peak in the critical Reynolds number range (Fig. 8). Lamont's C_Y/C_N results for $\varphi = 40$ deg are slightly above Keener's results for the same angle of attack, but are somewhat below Keener's peak $|C_Y|_{\max}/C_N$. More importantly, the data follow the same Reynolds number trend (Fig. 8).

In general, Lamont's ogive data are in agreement with results of Keener[23] for an $\ell/d = 3.5$ pointed ogive, verifying that the presence of the aft cylinder has little effect on the loads on the ogive, in agreement with earlier results.[23] However, isolated roughness spots in the nose-cylinder juncture can affect the total asymmetry development.[31-33] The shape of the $|C_Y|_{\max}/C_N$ curve for the $\ell/d = 3.5$ ogive in Fig. 8 is fairly typical for bodies dominated by a single side force cell. The peak is usually quite sharp, and it is often followed by an equally sharp minimum.

Lamont (in another publication) shows data for an ogive-cylinder in the critical Reynolds number range having a very small side force distributed along the entire body[21] (Fig. 9). He speculates that this occurs when the boundary layer on both sides of the body is transitional, and as for the 2D cylinder, irregular transition and separation breaks up the organized vortex shedding.[34-36] However, the axial flow component on the inclined cylinder should help organize the flow separation, as we have suggested,[3-6] and have an effect similar to the spanwise correlation accomplished in 2D flow when the amplitude of the translating oscillation exceeds a few percent of the cylinder diameter.[35] Thus, in the 3D case, organized critical separation should occur.

Figure 10 presents a logical progression of asymmetric vortex separation with increasing Reynolds number that explains how both a maximum and a minimum $|C_Y|_{\max}/C_N$ can occur in the critical Reynolds number range. At subcritical effective Reynolds numbers, asymmetric subcritical separation occurs near the 80 deg meridian to produce a moderate normalized side force. As the critical Reynolds number range is entered, critical/subcritical separation can occur. This provides the maximum differential in the separation location on opposite sides of the body ($\varphi = 80$ deg on one side and $\varphi = 140$ deg on the other) and the maximum suction pressure differential ($\Delta C_p \geq 1.2$, Fig. 3) in the vicinity of the lateral meridian where it is the most effective in producing a side force. The peak is sharp because a relatively small increase in Reynolds number results in asymmetric critical separation where nearly equal suction pressures occur at the lateral meridians and the separation asymmetry affects the pressures only at $\varphi = 140$ deg, where they are relatively ineffective in producing a side force. Thus, both the normalized side force and the side force itself will be very small (e.g. Fig. 9). This explains Lamont's small side force (Fig. 9) and the minimum normalized side force (Figs. 8 and 10). Finally, as R_{eff} increases through the supercritical regime on to the transcritical region, the flow separation asymmetry moves toward the lateral meridian where it is once again efficient in generating a side force.

This progressive change of the flow separation type from subcritical/subcritical through critical/subcritical to critical/critical has been observed on a 2D cylinder normal to the flow (Fig. 11).[16] At $R_d \leq 0.2 \times 10^6$, subcritical flow separation results in a base pressure of $C_{p_b} = -1.1$ and a normalized vortex shedding frequency of 0.19. At $R_d > 0.4 \times 10^6$, critical separation exists on both sides of the cylinder, resulting in $C_{p_b} = -0.23$ and $fd/U_\infty = 0.46$, all in agreement with the decreased wake size.[34] The experiment also showed that in a very narrow R_d region, just below $R_d = 0.4 \times 10^6$, critical separation is obtained only on one side, whereas the other side has subcritical flow separation, as is evidenced by the intermediate values of C_{p_b} and Strouhal number. Bearman measured $c_l = 1.3$, $c_d = 0.45$ at $R_d = 0.37 \times 10^6$, giving $c_l/c_d = 2.9$, which falls precisely on our boundary for c_{lp}/c_d (Ref. 2).

In summary, the results obtained recently by Keener and Lamont tend to support our postulation[1,2] that the peak normalized side force occurs in the critical R_{eff} range.

Effects of Body Motion

Vortex-induced side force is of concern for aircraft dynamics, as it produces a large side force near the nose at an angle of attack where the control surfaces are stalled or nearly stalled. Thus, spin will result if the side force overpowers the rudder. The effect on missiles can be equally disturbing at the high angles of attack at which many modern high performance weapons operate. Our earlier studies[4-6] indicated that there is

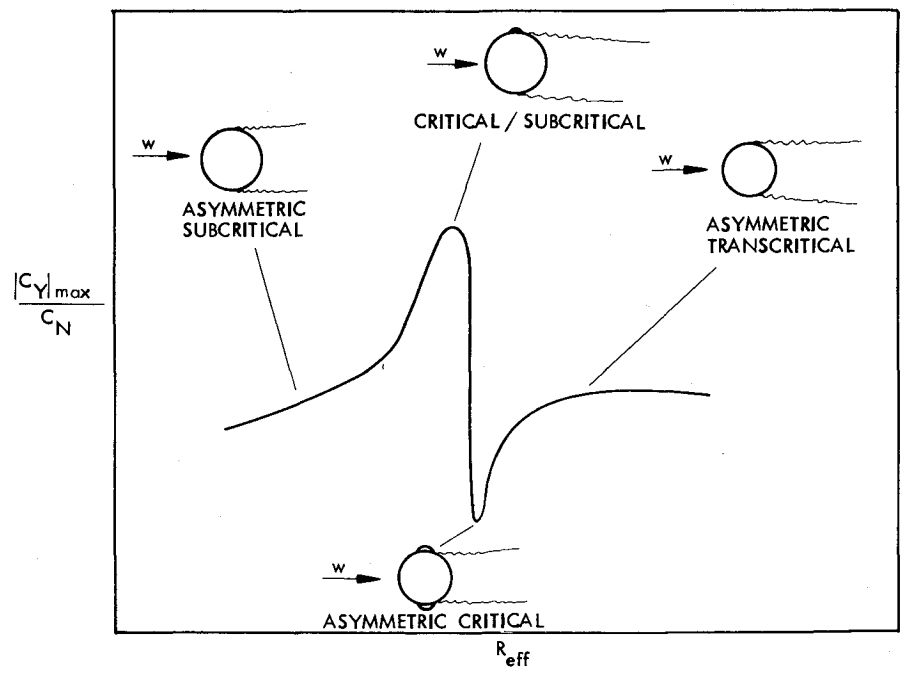

Fig. 10 Postulated effects of flow separation type on the maximum normalized side force.

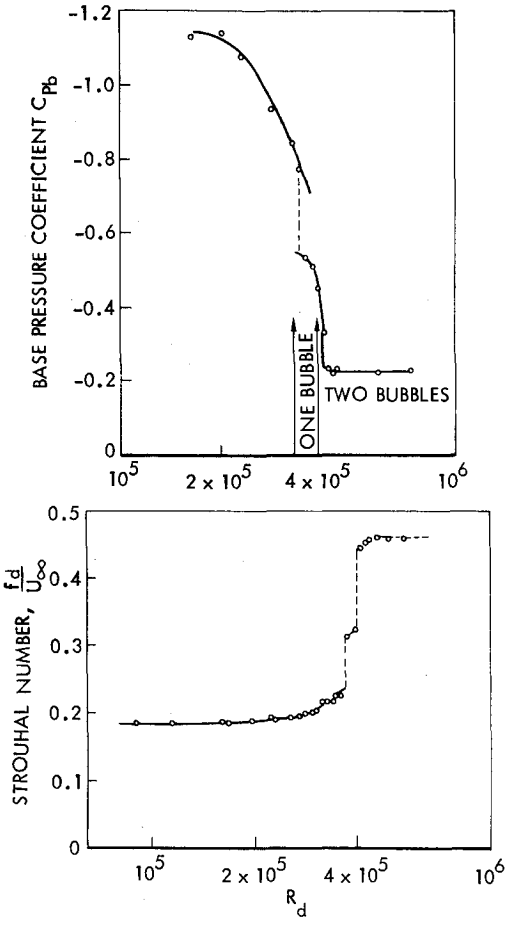

Fig. 11 Base pressure and Strouhal number in the wake of a circular cylinder (Ref. 16).

a strong coupling between body motion and flow separation which could cause a lock-in of the maximum vortex asymmetry. Recent experimental results[37] demonstrate the power of this coupling (Fig. 12). It was found that even though the static side force shows a preferred yawing direction, the model will spin in either direction if it is initially pushed lightly. Figure 12 shows that the two directions produce very much the same magnitude spin rate. That is, the motion overrides the static asymmetry, locking in the vortex asymmetry in a direction completely determined by the motion.

The mechanism that causes this driving asymmetry to lock in is the so-called moving wall effect described in Ref. 3 (Fig. 13). The no-slip conditions of the circumferential flow component at the windward meridian cause the boundary layer profile to be more filled out on the advancing side. The resulting turbulent-like boundary layer profile delays the separation on the advancing side of the body. On the retreating side, the effect is the opposite, promoting separation. The net result is that the coning motion reinforces the initial asymmetry and the associated side force, driving the motion (Fig. 13, Station F).

This is valid for the initial asymmetric vortex pair generated on the forebody. Aft of the coning axis however, the moving wall effects are reversed, and can reinforce the side moment only if a separate vortex pair exists over the aft body which is of the opposite sense compared to the forebody vortex pair (Fig. 13, Station A). Flow visualization shows that such a switch indeed takes place.[37]

In view of this large effect of the vehicle motion, it appears prudent to apply the peak normalized side force over the full Reynolds number range for the critical separation as we have done (Fig. 8). Although the peak value will only be realized at a discrete Reynolds number, statically[14] the coupling with the vehicle motion could cause the full scale dynamic aircraft or missile to lock in to the critical/subcritical asymmetry over a significant Reynolds number range.

Relaminarization

In the past, we have speculated[6] that accelerated flow effects over the convex surface of the ogive-cylinder shoulder could cause relaminarization of the boundary layer, thus delaying the natural progression from critical/subcritical separa-

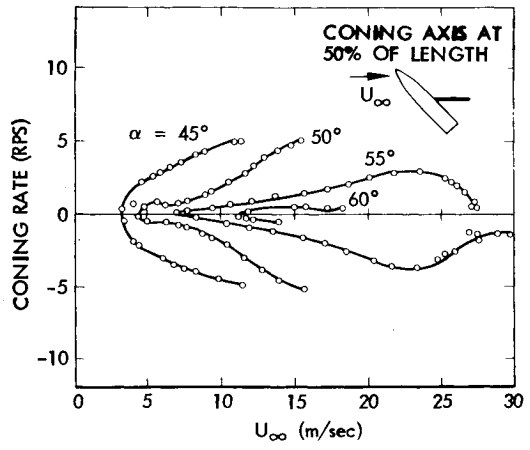

Fig. 12 Dual spin characteristics for a cone-cylinder (Ref. 37).

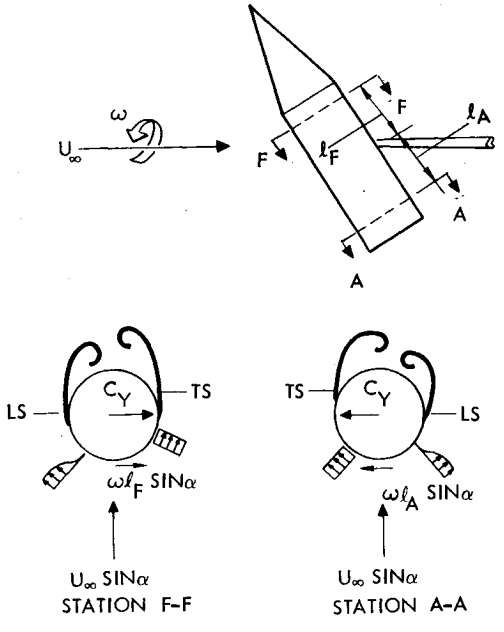

Fig. 13 Effect of body rotation on separation asymmetry in the critical Reynolds number range.

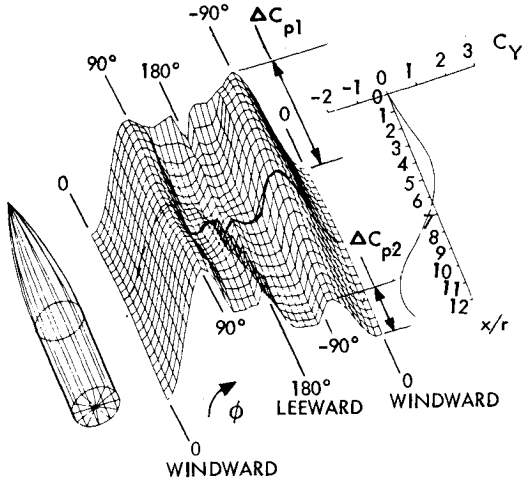

Fig. 14 Evidence of turbulent separation reverting to laminar separation $R_d = 1.25 \times 10^6$ (Ref. 29).

tion to asymmetric supercritical separation. There are now experimental data that indicate that the separation can degenerate to a lower Reynolds number type aft of the ogive-cylinder shoulder,[29] although we no longer believe it to be the main cause of the dip in the $|C_Y|_{max}/C_N$ curve.

Lamont's pressure data[29] for an ogive-cylinder show turbulent separation to occur on the ogive followed by laminar separation on the cylinder (Fig. 14). Even though the pressure scale has not been specified, one can see the suction pressure peaks develop near the lateral meridians (suction pressures are plotted upward) with a positive pressure recovery near the leeward meridian. Near the nose, the rapid pressure recovery indicative of flow separation occurs at roughly $\varphi = 110$ deg on the left side and $\varphi = 120$ deg on the right, indicating turbulent separation on both sides of the nose. On the right side, separation gradually moves outboard, occurring at $\varphi = 80$ deg at the end of the body. Simultaneously the suction peak is reduced roughly 50%, i.e., $\Delta C_{p_2} = 0.5\Delta C_{p_1}$ (Fig. 14). This, combined with the outboard movement of separation, is, we believe, indicative of a change from turbulent to laminar separation (compare with the 2D data in Fig. 3).[19] This shift from turbulent to laminar separation appears to be associated with the change in the sign of the side force (Fig. 14). The positive leeside pressure peak also moves from the $\varphi = 180$ deg meridian near the nose to between the $\varphi = 140$ deg and $\varphi = 100$ deg meridians on the aft right side of the body.

The reason for the switch from turbulent to laminar separation is presently unknown. We can conceive of two phenomena that might be responsible. They are presented herein as thought-provoking possibilities in an attempt to stimulate further research.

Based upon recent experimental results for the downstream effect of a roughness element located on the windward meridian of the nose,[33] one would conclude that the accelerated flow effects from the windward side expansive flow over the nose-cylinder shoulder could cause relaminarization of the flow downstream at the lateral meridian. The surface flow direction will vary from the axial direction along the windward meridian to being inclined at roughly 80 deg to the axis near the lateral meridian, where the flow separates. Thus, the axial pressure gradient can affect the windward boundary layer that eventually is carried around the body to influence the boundary layer character at separation. A similar degeneration of the separation type is also evident at a Reynolds number of 4×10^6 in Ref. 29.

The phenomenon appears to be associated with the shedding of a vortex, as the change of separation type correlates with a switch in the sign of the side force. Thus, an alternative (currently our preferred) explanation might be that the movement of the leeside stagnation point due to the shedding of a vortex may force the separation point of the following vortex to move circumferentially ahead of the location of transition in the crossflow plane, resulting in laminar separation. If this is the case, the effect should vanish at very high Reynolds numbers where transition occurs well upstream of the lateral meridian.

It is clear that the boundary layer transition plays a very important role in establishing the peak $|C_Y|_{max}/C_N$. There is also experimental evidence indicating that it can be the original source of the asymmetry, especially in the case of nonslender forebodies. Extreme care is therefore needed when applying subscale wind tunnel test results to full scale vehicle design. The results by Rau[38] and others[39] suggest that boundary layer tripping devices cannot be used on an ogive-cylinder to simulate full scale high angle of attack characteristics at subscale Reynolds numbers, as has been suggested.[40]

Conclusions

A critical review of recent experimental data lends further support for the postulation that the maximum normalized side force occurs in the critical Reynolds number range and is associated with critical/subcritical flow separation. A mini-

mum normalized side force appears to follow the maximum at a slightly higher Reynolds number, which we believe is due to asymmetric critical/critical vortex separation.

New experimental data have dramatically demonstrated that body motion can lock in a vortex asymmetry to cause self-induced coning. The fact that opposite vortex asymmetries are produced forward and aft of the coning axis, maximizing the driving moment, is most significant.

Other recent experiments seem to show that laminar vortex separation can occur aft of turbulent separation on a slender body at high angle of attack. This serves to underscore our limited understanding of the asymmetric vortex shedding phenomenon and the need for further research.

References

[1]Reding, J.P. and Ericsson, L.E., "Maximum Vortex-Induced Side Force," *Journal of Spacecraft and Rockets*, Vol. 15, July-Aug. 1978, pp. 201–207.

[2]Reding, J.P. and Ericsson, L.E. "Maximum Side Forces and Associated Yawing Moments on Slender Bodies," *Journal of Spacecraft and Rockets*, Vol. 17, Nov.-Dec. 1980, pp. 515–521.

[3]Ericsson, L.E. and Reding, J.P., "Steady and Unsteady Vortex-Induced Loads on Slender Vehicles," *Journal of Spacecraft and Rockets*, Vol. 18, March-April 1981, pp. 97–109.

[4]Ericsson, L.E. and Reding, J.P., "Review of Vortex-Induced Asymmetric Loads—Part I," *Z. Flugwiss. Weltraumforsch.*, 5, 1981, Heft 3, pp. 162–174.

[5]Ericsson, L.E. and Reding, J.P., "Review of Vortex-Induced Asymmetric Loads—Part II," *Z. Flugwiss. Weltraumforsch.*, 5, 1981, Heft 6, pp. 349–366.

[6]Ericsson, L.E. and Reding, J.P., "Vortex-Induced Asymmetric Loads in 2-D and 3-D Flows," AIAA Paper No. 80-0181, Jan. 1980.

[7]Clark, W.C., "Body Vortex Formation on Missiles in Incompressible Flows," AIAA Paper No. 77-1154, Aug. 1977.

[8]Reding, J.P. and Ericsson, L.E., "Maximum Vortex-Induced Side Forces on Slender Bodies at High Angle of Attack," High Angle of Attack Aerodynamic Working Group Meeting, Redstone Arsenal, Ala., Feb. 1977.

[9]Ericsson, L.E. and Reding, J.P., "Vortex-Induced Asymmetric Loads on Slender Vehicles," LMSC-D630807, Jan. 1979.

[10]Achenbach, E., "Influence of Surface Roughness on the Cross-Flow Around a Circular Cylinder," *Journal of Fluid Mechanics*, Vol. 46, Part 2, 1971, pp. 321–335.

[11]Ericsson, L.E., "Aeroelastic Instability Caused by Slender Payloads," *Journal of Spacecraft and Rockets*, Vol. 4, Jan. 1967, pp. 65–73.

[12]Achenbach, E., "Distribution of Local Pressure and Skin Friction Around a Circular Cylinder in Cross-Flow up to $Re = 5 \times 10^2$," *Journal of Fluid Mechanics*, Vol. 34, Part 4, 1968, pp. 625–639.

[13]Jones, G.W., Jr., Cincotta, J., and Walker, W., "Aerodynamic Forces on a Stationary and Oscillating Circular Cylinder at Very High Reynolds Number," NASA TR-300, Feb. 1969.

[14]Ericsson, L.E. and Reding, J.P., "Dynamic Stall Simulation Problems," *Journal of Aircraft*, Vol. 8, July 1971, pp. 579–583.

[15]Humphreys, J.S., "On a Circular Cylinder in a Steady Wind at Transition Reynolds Numbers," *Journal of Fluid Mechanics*, Vol. 9, Part 4, 1960, pp. 603–612.

[16]Bearman, P.W., "On Vortex Shedding from a Circular Cylinder in the Critical Reynolds Number Regime," *Journal of Fluid Mechanics*, Vol. 37, Part 3, 1969, pp. 577–585.

[17]Kamiya, N., Suzenky, S., and Mishi, T., "On the Aerodynamic Forces Acting on a Circular Cylinder in the Critical Range of the Reynolds Number," AIAA Paper No. 79-1475, July 1979.

[18]Dahlem, V. and Sjereden, D., Private communication of unpublished MX wind tunnel data, Flight Dynamics Laboratory, Wright-Patterson Air Force Base, Ohio, 2 May 1978 and 20 Aug. 1978.

[19]Horner, S.F., *Fluid Dynamic Drag*, Book published by the author, 1958.

[20]Jorgensen, L.H., "Prediction of Static Aerodynamic Characteristics for Space Shuttle Like and Other Bodies at Angles of Attack from 0° to 180°," NASA TN D-6996, Jan. 1973.

[21]Lamont, P.J., "Pressure Measurements on an Ogive-Cylinder at High Angles of Attack with Laminar, Transitional or Turbulent Separation," AIAA Paper No. 80-1556, 1980.

[22]Chapman, G.T., Keener, E.R., and Malcolm, G., "Asymmetric Aerodynamic Forces on Aircraft Forebodies at High Angles of Attack—Some Design Guides," Paper No. 16, AGARD Meeting on Stall/Spin Problems of Military Aircraft, Ames Research Center, Moffett Field, Calif., Nov. 18-21, 1976.

[23]Keener, E.R. and Chapman, G.T., "Onset of Aerodynamic Side Forces at Zero Sideslip on Symmetric Forebodies at High Angles of Attack," AIAA Paper No. 74-0770, Aug. 1974.

[24]Keener, E.R. and Taleghani, J., "Wind Tunnel Investigations of the Aerodynamic Characteristics of Five Forebody Models at High Angles of Attack at Mach Numbers from 0.25 to 2," NASA TM X-73, 076, Dec. 1975.

[25]Keener, E.R., Chapman, G.T., Cohen, L., and Taleghani, J., "Side Forces on a Tangent-Ogive Forebody with a Fineness Ratio of 3.5 at High Angles of Attack and Mach Numbers from 0.1 to 0.7," NASA TM-3437, Feb. 1977.

[26]Keener, E.R., Chapman, G.T., Cohen, L., and Taleghani, J., "Side Forces on Forebodies at High Angles of Attack and Mach Numbers from 0.1 to 0.7. Two Tangent Ogives, Paraboloid and Cone," NASA TM-3438, Feb. 1977.

[27]Keener, E.R., "Oil-Flow Separation Patterns on an Ogive Forebody," *AIAA Journal*, Vol. 21, April 1983, pp. 550–556.

[28]Atraghji, E.G., "The Influence of Mach Number, Semi-Nose Angle and Roll Rate on the Development of the Forces and Moments over a Series of Long Slender Bodies of Revolution at Incidence," NAE Data Report 545/0020, 1967, National Research Establishment, Ottawa, Canada.

[29]Lamont, P.J., "The Complex Asymmetric Flow Over a 3.4D Ogive Nose and Cylindrical Afterbody at High Angles of Attack," AIAA Paper No. 82-0053, Jan. 1982.

[30]Hunt, B.L., "Asymmetric Vortex Forces and Wakes on Slender Bodies," AIAA Paper No. 82-1336, Aug. 1982.

[31]Kruse, R.T., Keener, E.R., Chapman, G.T., and Classer, G., "Investigation of the Asymmetric Aerodynamic Characteristics of Cylindrical Bodies of Revolution with Variations in Nose Geometry and Rotational Orientation at Angles of Attack to 58° and Mach Numbers to 2.0," NASA TM 78533, Sept. 1979.

[32]Robinson, M.L., "The Attachment Line Boundary Layer on a Body at Incidence in Subsonic Flow," *Proceedings of Fluid Mechanics Conference*, Brisbane, Australia, 18-22 Aug. 1980, pp. 549–552.

[33]Robinson, M.L., "Effects of Singular Roughness Element," private communication of unpublished experimental results, Lockheed Missiles & Space Company, Inc., Sunnyvale, Calif., 11 Oct. 1982.

[34]Ericsson, L.E. and Reding, J.P., "Criterion for Vortex Periodicity in Cylinder Wakes," *AIAA Journal*, Vol. 17, Sept. 1979, pp. 1012–1013.

[35]Ericsson, L.E., "Karman Vortex Shedding and the Effect of Body Motion," *AIAA Journal*, Vol. 18, Aug. 1980, pp. 935–944.

[36]Ogawa, A. and Nakagawa, K., "Stability of the Vortex Street in the Wake of Stationary and Vibrating Cylinders," *Transactions of the Japan Society, Aerospace Science*, Vol. 20, Feb. 1978, pp. 167–176.

[37]Yoshinaga, T., Tate, A., and Inoue, K., "Coning Motion of Slender Bodies at High Angles of Attack in Low Speed Flow," AIAA Paper No. 81-1899, Aug. 1981.

[38]Rau, D.M., "Side-Force Alleviation on Slender, Pointed Forebodies at High Angles of Attack," *Journal of Aircraft*, Vol. 16, Nov. 1979, pp. 763–768.

[39]Ericsson, L.E. and Reding, J.P., "Alleviation of Vortex-Induced Asymmetric Loads," *Journal of Spacecraft and Rockets*, Vol. 17, Nov.-Dec. 1980, pp. 546–553.

[40]Poll, D.I.A., "Some Effects of Boundary Layer Transition on Slender Axi-Symmetric Bodies at Incidence in Incompressible Flow," Paper 13, AGARD Symposium on Missile Aerodynamics, Trondheim, Norway, 20-22 Sept. 1982.